BosonSampling with Controllable Distinguishability

Max Tillmann[1], Si-Hui Tan[2], Sarah E. Stoeckl[1], Barry C. Sanders[3], Hubert de Guise[4], René Heilmann[5], Stefan Nolte[5], Alexander Szameit[5], Philip Walther[1]
[1]*Faculty of Physics, University of Vienna, Boltzmanngasse 5, A-1090 Vienna, Austria*
[2]*Singapore University of Technology and Design, 20 Dover Drive, 138682 Singapore*
[3]*Institute for Quantum Science and Technology, University of Calgary, Alberta, Canada T2N 1N4*
[4]*Department of Physics, Lakehead University, Thunder Bay, Ontario, P7B 5E1, Canada and*
[5] *Institute of Applied Physics, Abbe Center of Photonics, Friedrich-Schiller Universität Jena, Max-Wien-Platz 1, D-07743 Jena, Germany*

Photonic BosonSampling computers[1] have inspired significant interest[2–5] because they have the potential to solve computationally hard problems efficiently using only a few–dozen indistinguishable photons. However, their ability to outperform classical computers is currently limited by their tight error tolerance[6, 7]. Whereas practical BosonSampling computation depends on the quality of the apparatus it is the photons distinguishability which is the fundamentally limiting source of error. Here we develop a method describing the transition probabilities of photons with arbitrary distinguishability through any linear–optical network. We test this experimentally by tuning the temporal delay of the input–photons. Our approach provides tighter estimates for the underlying BosonSampling distribution by relating the output to the transition matrix immanants[8], enabling the main source of errors to be quantified. This is essential for experimentally realizable implementations. Our method may enable generalized BosonSampling computation through the use of immanants and not just permanents.

I. INTRODUCTION

BosonSampling processes n identical simultaneous bosons, e.g. photons, through a randomly chosen passive linear network and yields an output distribution relying on non–classical interference[9]. Such samplings cannot be efficiently simulated on conventional computers, due to two reasonable conjectures: the Permanent–of–Gaussians conjecture and the Permanent Anti–Concentration Conjecture. Furthermore the existence of a classical polynomial-time randomized algorithm would imply a major collapse of the computational complexity polynomial hierarchy.
The improbability of such a collapse indicates instead that efficient approximate experimental BosonSampling would falsify the extended Church–Turing thesis. This thesis states that problems efficiently solvable by physical devices are also solvable efficiently by a probabilistic, but non–quantum, Turing machine. Consequently efficiently scalable experimental BosonSampling would present strong evidence that quantum computing is superior to classical computing based on probabilistic Turing machines.

The importance of experimentally testing the superiority of quantum computing over classical computing has been the impetus of several impressive photon interferometry experiments using integrated[3–5] and fiber–based systems[2]. These experimental benchmarks of optical BosonSampling stimulated discussions[10, 11] whether BosonSampling output distributions can be discriminated from uniform distributions in the large photon–number regime. Recent experimental comparisons[12, 13] of output distributions originating from classical and quantum multi–photon interference strongly indicate that output distributions from BosonSampling computers are not uniform. However, for more accurate studies the influence of errors, which is still under investigation[14–16], needs to be assessed.
Aaronson and Arkhipov, in their seminal theoretical introduction of the BosonSampling problem and its potential implementation, presciently identified five "obvious" errors that have to be considered in experimentally realizing BosonSampling. These errors are: imperfect preparation of the n–photon Fock–state, inaccurate description of the interferometer, photon losses, imperfect detectors and non–simultaneity of photon arrival times. Photon losses and imperfect detection can be ameliorated for demonstrations of principle by post–selection techniques, and inaccuracy of the description of the transition matrix can be minimized by stabilisation and process tomography.
Consequently imperfect preparation of photons and non–simultaneity are the most insidious of the five problems and need careful study. State of the art multi–photon sources face intrinsic challenges in terms of their photons' distinguishability and well–defined photon number states, both affecting crucially the performance of BosonSampling computers. Photon–number–resolving detectors with near unit detection efficiency[17–19] provide the quantum technology for heralding precise photon–number input states[20], rendering one source of imperfection rather unlikely in the near future. In contrast the achievement of indistinguishable photons is still experimentally demanding by requiring precise control of various parameters such as spectral–, temporal–, spatial– and polarization properties[21]. In the classical case of all photons being distinguishable the resulting output distribution of a sampling–computer can always be efficiently calculated on a conventional computer.

In this work we manipulate the distinguishability of

single photons by controlling their relative time delays. Here we construct a theoretical framework capable of determining the quality of BosonSampling for arbitrary degrees of distinguishability. Our approach contrasts with all previous experiments that considered only the extreme cases of perfect classical or quantum conditions. We further show that the output distribution depends not only on the permanent - as in the case of an ideal BosonSampling computation. It rather depends on all immanants of the interferometer transition matrix for the specific representations given by the number of the input photons n and the number of modes m.

The simplest instance of BosonSampling is the Hong–Ou–Mandel dip[22], wherein two photons are injected into distinct input ports of a beam splitter, which is effectively an $n = m = 2$ interferometer. One element of the output probability distribution, the case where the two photons exit the beam splitter in different output ports, is recorded via a coincidence measurement. This coincidence rate depends on the transformation matrix, here defined by the splitting ratio of the beam splitter, and the distinguishability of the photons. In the iconic example of a balanced, i.e. 50/50, beam splitter and indistinguishable photons the coincidence rate vanishes. The established technique to calibrate for the point of maximal non–classical interference relies on tuning the relative temporal delay, i.e. the distinguishability between the two photons. Mathematically the relevant function is an overlap integral, which accounts for the photons' key properties such as spectral shape, polarization, spatial mode and relative temporal delay. Any distinguishability due to causes other than delay can be treated as mode mismatch, which reduces non–classical interference according to this mode–overlap integral. The coincidence rate for an arbitrary beam splitter described by a transformation unitary B corresponds to

$$P_{11}(\Delta\tau) = \frac{1}{2}\left(|\mathrm{per}(B)|^2 + |\det(B)|^2\right) + \zeta \mathrm{e}^{-\xi\Delta\tau^2}\left(|\mathrm{per}(B)|^2 - |\det(B)|^2\right),$$

where $0 \leq \zeta \leq 1$ is derived from the mode–overlap integral and ξ is a factor describing the shape of the interference feature (see supplementary information for further details). The permanent (per) and determinant (det) are special cases of the immanant, $\mathrm{imm}(M) = \sum_\sigma \chi(\sigma) \prod_i M_{i\sigma(i)}$ for M_{ij} matrix elements of M, with $\chi(\sigma)$ the character of permutation σ: $\chi(\sigma) = 1$ for the permanent and $\chi(\sigma) = \mathrm{sgn}(\sigma)$ for the determinant. For perfect mode matching, $P_{11}(0) = |\mathrm{per}(B)|^2$, which is zero for a balanced beam splitter. Controllable distinguishability can thus be understood as varying the relative weights of $|\mathrm{per}(B)|^2$ and $|\det(B)|^2$ in equation (I). This weighting of permanent and determinant in the coincidence rate generalizes to relative weightings of immanants for more than two modes[23, 24].

II. EXPERIMENT

Photonic BosonSampling extends such non–classical interference to more photons n and even larger interferometric networks with $m > n$ channels. We implement such a network for $n = 3$ and $m = 5$, and test the effect of distinguishability by controlling relative time delays between the three photons. Coincidences are measured at three of the five output ports as a function of the relative delays $\Delta\tau_1$ between the first and second photon and $\Delta\tau_2$ between the second and third photon. There exist ten possible ways of injecting three photons into a five–moded interferometer and similarly ten different ways for the three photons to exit this network, resulting in 100 different combinations of input and output ports. Each combination specifies a 3×3 submatrix R and the coincidence rates, given by equation (1), of this scattering event can be visualized as a three–dimensional landscape with the $(\Delta\tau_1, \Delta\tau_2)$ plane serving as the domain. In the limit $\Delta\tau_1 = \Delta\tau_2 = 0$ and perfect indistinguishability the ten landscapes for one input combination collapse to the ten post–selected probabilities of a BosonSampling output distribution. The coincidence rate of each landscape corresponds to

$$\begin{aligned} P_{111}(\Delta\tau_1, \Delta\tau_2) &= \int d\omega \int d\omega' \int d\omega'' |\langle\psi_{in}|\hat{R}^\dagger \hat{a}_1^\dagger(\omega)\hat{a}_2^\dagger(\omega')\hat{a}_3^\dagger(\omega'')|0\rangle|^2 \qquad (1) \\ &= \boldsymbol{v}^\dagger\big(\mathbb{1} + \varrho_{12}\zeta_{12}\mathrm{e}^{-\xi_{12}\Delta\tau_1^2} + \varrho_{23}\zeta_{23}\mathrm{e}^{-\xi_{23}\Delta\tau_2^2} \\ &\quad + \varrho_{13}\zeta_{13}\mathrm{e}^{-\xi_{13}(\Delta\tau_1-\Delta\tau_2)^2} + \varrho_{123}\zeta_{123}\left(\mathrm{e}^{-\xi_{123}(\Delta\tau_1,\Delta\tau_2)} + \mathrm{e}^{-\xi^*_{123}(\Delta\tau_1,\Delta\tau_2)}\right)\big)\boldsymbol{v}, \qquad (2) \end{aligned}$$

where R denotes a transformation by a 3×3 submatrix and $\hat{a}_1^\dagger(\omega)$, $\hat{a}_2^\dagger(\omega')$ and $\hat{a}_3^\dagger(\omega'')$ the creation operators in modes $1, 2$, and 3 for photons with different spectral

shape functions dependent on the frequency variables $\omega, \omega', \omega''$. An expression of equation (1), expanded in terms of immanants, determinants and permanents, results in a linear superposition of 60 terms. However, choosing a different decomposition allows a compact presentation as shown in equation (2) (see methods and supplementary information for further details). Here the immanants, permanent and determinant are contained in a six–dimensional vector $\boldsymbol{v}$. Analogous to equation (I) ζ terms are derived from the mode–overlap integral and ξ terms are factors describing the shape of the interference feature. The subscripts label the input modes of the photons, and ϱ_{12},ϱ_{13},ϱ_{23} and ϱ_{123} are permutation matrices describing the symmetry under exchange of the photons.

Distinct regions in a landscape are related to different physical behavior of the three photons (see Fig. 1). In the center ($\Delta\tau_1 = \Delta\tau_2 = 0$), all photons exhibit maximal indistinguishability and the output probability distribution is predominantly proportional to the permanent. Any distinguishability, for example due to polarization or spectral mode–mismatch, leads to contributions from immanants and the determinant, even for perfect temporal overlap. This is reflected in equation (2) by the weighting factors ζ being smaller than one. Note that only perfect indistinguishability causes destructive interference of 54 of the 60 terms such that only the contribution from the permanent will show up in the output distribution.
Outside the central region, three troughs or ridges of pairwise temporal indistinguishability ($\Delta\tau_1 = \Delta\tau_2$, $\Delta\tau_1 = 0$, and $\Delta\tau_2 = 0$) structure the landscape further. These emerge as a result of non–classical interference between two of the three photons. The output probability distribution is now a sum containing the permanent, determinant and some immanants. The weighting of those is dominated by the temporal overlap dependent on $\Delta\tau_1$ and $\Delta\tau_2$, whereas the weighting factors ζ are small in comparison. Note that contributions from the determinant appear for partial distinguishability of all interfering photons only, originating for example from modal mismatch.
The remaining areas form plateaux, where all photons exhibit complete temporal distinguishability. Here the temporal overlap functions converge to zero which renders the output probability completely independent of any weighting factors, often referred to as classical behaviour of the photons.

III. CONCLUSION

In Fig. 1 we illustrate the central result of our experiment. We sampled the output probability for six different sets of temporal delays, and therefore distinguishability, for two different combinations of output modes (see supplementary information for detailed information). The predicted output probabilities are calculated from the reconstruction of the unitary matrix describing the interferometer. We find a reduced χ^2 of 1.38 and 1.10 for the two different combinations of output modes. Small deviations from the model can be attributed to higher–order emission, the influence of loss and inaccuracy in the reconstructed description of the interferometric network. Our method allows the influence of photon distinguishability to be quantified and is independent of the source of the distinguishability. It is universally applicable to any linear–optical network processing single–photons and exhibiting non–classical interference. By relating the probability distributions to the transition matrix immanants tighter estimates for the underlying BosonSampling distribution can be achieved. Our method is not only valuable for assessing the quality of a BosonSampling computer but also shows a way to expand intermediate computations to more general sampling problems based on immanants.

IV. METHODS

Three–photon coincidence probability Vector $\boldsymbol{v}$ in equation (2) is defined as:

$$\boldsymbol{v} = \begin{pmatrix} \mathrm{per}(R) \\ \det(R) \\ \frac{1}{2\sqrt{3}}\mathrm{imm}(R) + \frac{1}{2\sqrt{3}}\mathrm{imm}(R_{312}) \\ \frac{1}{6}\mathrm{imm}(R) - \frac{1}{3}\mathrm{imm}(R_{132}) - \frac{1}{6}\mathrm{imm}(R_{213}) + \frac{1}{3}\mathrm{imm}(R_{312}) \\ \frac{1}{6}\mathrm{imm}(R) + \frac{1}{3}\mathrm{imm}(R_{132}) + \frac{1}{6}\mathrm{imm}(R_{213}) + \frac{1}{3}\mathrm{imm}(R_{312}) \\ -\frac{1}{2\sqrt{3}}\mathrm{imm}(R) + \frac{1}{2\sqrt{3}}\mathrm{imm}(R_{213}) \ , \end{pmatrix} \tag{3}$$

where R_{ijk} is R with rows arranged in order i, j and k.

State generation A Ti–Sapphire oscillator emitting 150 fs pulses at 789 nm and a repetition rate of 80 MHz is frequency doubled in a LiB_3O_5 (LBO) crystal (see Fig. 2 for a schematic of the experimental setup). The output

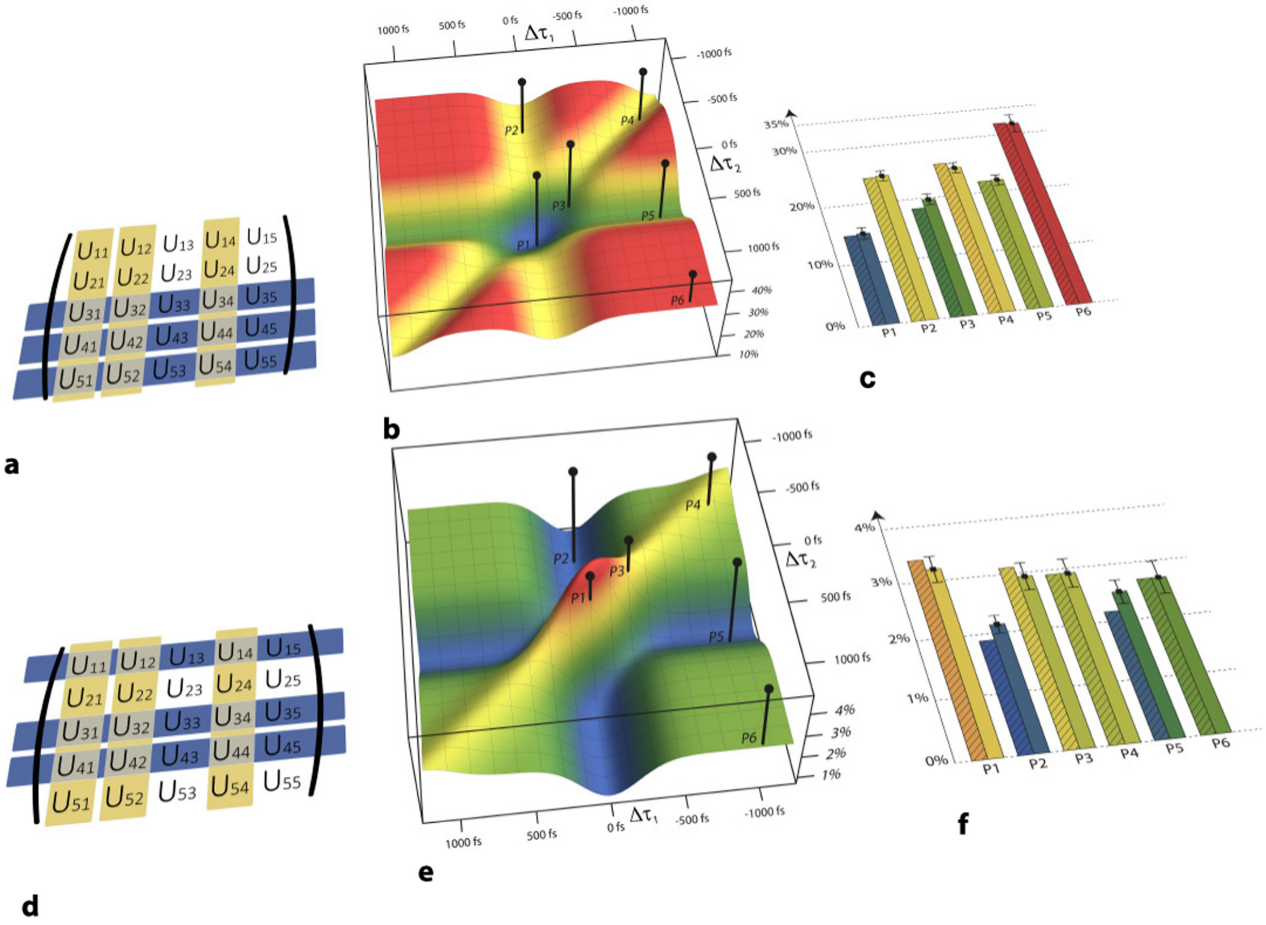

Figure 1. **Three–photon coincidence landscapes** Three photons enter the interferometric network, one each in mode 1, 2 and 4 (highlighted in yellow), and exit the network in modes **a)** 3, 4 and 5 and **d)** 1, 3 and 4 respectively (highlighted in blue). The intersections of the inputs' columns and the outputs' rows uniquely select matrix–entries that constitute 3×3 submatrices. Tuning the temporal delay of the three photons with respect to each other ($\Delta\tau_1$ and $\Delta\tau_2$) gives rise to coincidence landscapes (**b)** and **e)**). Their temporal distinguishability determines the degree of non–classical interference and therefore probability to detect such an event. Six characteristic points (P1 ... P6) of each landscape are experimentally sampled. Theoretical prediction (left bars, shaded) and experimentally obtained output probabilities (right bars) for the six points and both output combinations are shown in **c)** and **f)**. The reduced χ^2 is 1.38 and 1.10 respectively and the experimental errors are calculated as standard deviation of the mean.

power of this second harmonic generation can be controlled by a power regulation stage consisting of a half–wave plate (HWP) and a polarizing beam splitter (PBS) placed before the LBO-crystal. The resulting emission at 394.5 nm is focused into a 2 mm thick β–BaB_2O_4 (BBO) crystal cut for degenerate non–collinear type–II down–conversion[25]. A compensation scheme consisting of HWPs and 1 mm thick BBO–crystals is applied for countering temporal and spatial walk–off. The two spatial outputs of the down–converter pass through narrowband interference filters ($\lambda_{\mathrm{FWHM}} = 3$ nm) to achieve a coherence time greater than the birefringent walk–off due to group velocity mismatch in the crystal ($|v_{g_e} - v_{g_o}|$ $\times$ half crystal thickness). Additionally this renders the photons close to spectral indistinguishability. The down–conversion–source is aligned to emit the maximally entangled Bell–state $|\phi^+\rangle = \frac{1}{\sqrt{2}}(|HH\rangle + |VV\rangle)$ when pumped at 205 mW cw–equivalent pump power. The state is coupled into single mode fibers (Nufern 780–HP) equipped with pedal–based polarisation controllers to counter any stress–induced rotation of the polarisation inside the fiber.

Each of these spatial modes is then coupled to one input of a PBS while its other input is occupied with a vacuum–state. The outputs pass HWPs and are subsequently coupled to four polarisation maintaining fibers (Nufern PM780–HP). Temporal overlap is controlled by two motorized delay lines that exhibit a bidirectional repeatability of $\pm$ 1 µm. Temporal alignment precision is limited by other factors in the setup to approximately $\pm$ 5 µm and is therefore within a precision of 2.5 % of the coherence length of the photons. The polarisation main-

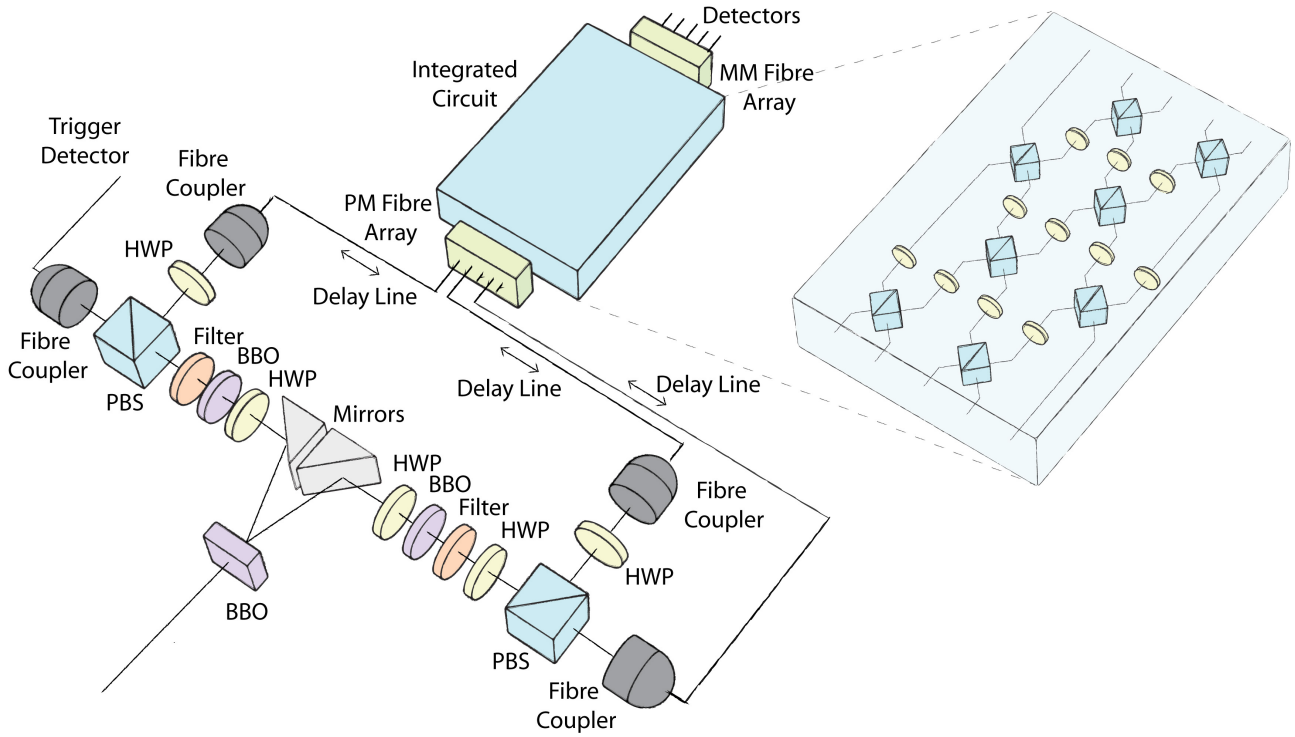

Figure 2. **Experimental setup.** Four photons are generated via spontaneous parametric down–conversion (SPDC) and distributed to four spatial modes with two PBSs. A four–fold coincidence event consisting of three photons exiting the network and a trigger event postselects the desired input state. The delay lines allow to tune the distinguishability and therefore quantum–interference of the three photons propagating through the waveguide. The integrated circuit is shown in a Mach–Zehnder–decomposition and consists of eight beam splitters and eleven phase shifters.

taining fibers are mated to a single mode fiber v–groove–array (Nufern PM780–HP) with a pitch of 127 µm and butt–coupled to the integrated circuit. The coupling is controlled by a manual six–axis flexure stage and stable within 5 % of the total single–photon counts over 12 hours. The output fiber array consists of a multimode v–groove–array (GIF–625) and the photons are detected by single–photon avalanche photodiodes which are recorded with a home–built Field Programmable Gate Array logic. The coincidence time window was set to 3 ns.
In order to measure the six points of the coincidence landscapes a three–photon input state was injected into the integrated network (see supplementary information for further details). Therefore the BBO was pumped with cw-equivalent power of 700 mW and the ratio of the six–photon emission over the desired four–photon emission was measured to be below 5 %.

Integrated network fabrication. The integrated photonic networks were fabricated using a femtosecond direct–write writing technology[26, 27]. Laser pulses were focused 370 µm below the surface of a high–purity fused silica wafer by an NA = 0.6 objective. The 200 nJ pulses exhibit a pulse duration of 150 fs at 100 kHz repetition rate and a central wavelength of 800 nm. In order to write the individual waveguides the wafer was translated with a speed of 6 cm/s. The waveguide modes exhibit a mode field diameter of 21.4 µm × 17.2 µm for a wavelength of 789 nm and a propagation loss of 0.3 dB/cm. This results in a coupling loss of −3.5 dB with the type of input fibers used in this experiment. Coupling to the output array results in negligible loss due to the use of multimode fibers.

[1] Aaronson, S. & Arkhipov, A. The computational complexity of linear optics. In *Proceedings of the 43rd annual ACM symposium on Theory of computing*, 333–342 (ACM, 2011).
[2] Broome, M. A. *et al.* Photonic boson sampling in a tunable circuit. *Science* **339**, 794–798 (2013).
[3] Spring, J. B. *et al.* Boson sampling on a photonic chip. *Science* **339**, 798–801 (2013).
[4] Tillmann, M. *et al.* Experimental boson sampling. *Nature Photonics* **7**, 540–544 (2013).
[5] Crespi, A. *et al.* Integrated multimode interferometers with arbitrary designs for photonic boson sampling. *Na-*

ture Photonics (2013).
[6] Rohde, P. P. & Ralph, T. C. Error tolerance of the boson-sampling model for linear optics quantum computing. *Physical Review A* **85**, 022332 (2012).
[7] Rohde, P. P., Motes, K. R., Knott, P. & Munro, W. J. Will boson-sampling ever disprove the extended church-turing thesis? *arXiv preprint arXiv:1401.2199* (2014).
[8] Littlewood, D. E. & Richardson, A. R. Group characters and algebra. *Philosophical Transactions of the Royal Society of London. Series A, Containing Papers of a Mathematical or Physical Character* **233**, 99–141 (1934).
[9] Metcalf, B. J. *et al.* Multiphoton quantum interference in a multiport integrated photonic device. *Nature communications* **4**, 1356 (2013).
[10] Gogolin, C., Kliesch, M., Aolita, L. & Eisert, J. Boson-sampling in the light of sample complexity. *arXiv preprint arXiv:1306.3995* (2013).
[11] Aaronson, S. & Arkhipov, A. Bosonsampling is far from uniform. *arXiv preprint arXiv:1309.7460* (2013).
[12] Spagnolo, N. *et al.* Efficient experimental validation of photonic boson sampling. *arXiv preprint arXiv:1311.1622* (2013).
[13] Carolan, J. *et al.* On the experimental verification of quantum complexity in linear optics. *arXiv preprint arXiv:1311.2913* (2013).
[14] Leverrier, A. & García-Patrón, R. Does boson sampling need fault-tolerance? *arXiv preprint arXiv:1309.4687* (2013).
[15] Rohde, P. P. & Ralph, T. C. Error tolerance of the boson-sampling model for linear optics quantum computing. *Physical Review A* **85**, 022332 (2012).
[16] Rohde, P. P. Optical quantum computing with photons of arbitrarily low fidelity and purity. *Physical Review A* **86**, 052321 (2012).
[17] Lita, A. E., Miller, A. J. & Nam, S. W. Counting near-infrared single-photons with 95% efficiency. *Optics express* **16**, 3032–3040 (2008).
[18] Zhou, Z. *et al.* Superconducting series nanowire detector counting up to twelve photons. *arXiv preprint arXiv:1311.6458* (2013).
[19] Marsili, F. *et al.* Detecting single infrared photons with 93% system efficiency. *Nature Photonics* **7**, 210–214 (2013).
[20] Ramelow, S. *et al.* Highly efficient heralding of entangled single photons. *Optics express* **21**, 6707–6717 (2013).
[21] Eisaman, M., Fan, J., Migdall, A. & Polyakov, S. Invited review article: Single-photon sources and detectors. *Review of Scientific Instruments* **82**, 071101–071101 (2011).
[22] Hong, C., Ou, Z. & Mandel, L. Measurement of subpicosecond time intervals between two photons by interference. *Physical Review Letters* **59**, 2044–2046 (1987).
[23] Tan, S.-H., Gao, Y. Y., de Guise, H. & Sanders, B. C. Su(3) quantum interferometry with single-photon input pulses. *Phys. Rev. Lett.* **110**, 113603 (2013). URL `http://link.aps.org/doi/10.1103/PhysRevLett.110.113603`.
[24] de Guise, H., Tan, S.-H., Poulin, I. P. & Sanders, B. C. Immanants for three-channel linear optical networks. *arXiv preprint arXiv:1402.2391* (2014).
[25] Kwiat, P. G. *et al.* New high-intensity source of polarization-entangled photon pairs. *Physical Review Letters* **75**, 4337 (1995).
[26] Itoh, K., Watanabe, W., Nolte, S. & Schaffer, C. B. Ultrafast processes for bulk modification of transparent materials. *MRS bulletin* **31**, 620–625 (2006).
[27] Marshall, G. D. *et al.* Laser written waveguide photonic quantum circuits. *Optics Express* **17**, 12546–12554 (2009).

ACKNOWLEDGMENTS

The authors thank I. Dhand and J. Cotter for helpful discussions and M. Tomandl for assistance with the illustrations. M.T., S.E.S. and P.W. acknowledge support from the European Commission with the project EQuaM -Emulators of Quantum Frustrated Magnetism (No 323714), GRASP - Graphene-Based Single-Photon Nonlinear Optical Devices (No 613024), PICQUE - Photonic Integrated Compound Quantum Encoding (No 608062), QuILMI - Quantum Integrated Light Matter Interface (No 295293) and the ERA-Net CHIST-ERA project QUASAR - Quantum States: Analysis and Realizations, the German Ministry of Education and Research (Center for Innovation Competence program, grant 03Z1HN31), the Vienna Center for Quantum Science and Technology (VCQ), the Austrian Nano-initiative Nanostructures of Atomic Physics (NAP-PLATON), and the Austrian Science Fund (FWF) with the projects PhoQuSi Photonic Quantum Simulators (Y585-N20) and the doctoral programme CoQuS Complex Quantum Systems, the Vienna Science and Technology Fund (WWTF) under grant ICT12-041, and the Air Force Office of Scientific Research, Air Force Material Command, United States Air Force, under grant number FA8655-11-1-3004. B.C.S. acknowledges support from AITF (Alberta Innovates Technology Futures), NSERC (Natural Sciences and Engineering Research Council), and CIFAR (Canadian Institute for Advanced Research). The work of H.dG. is supported in part by NSERC of Canada. S.-H.T. acknowledges support from the Singapore National Research Foundation under NRF Award No. NRF-NRFF2013-01. R.H., S.N. and A.S. acknowledge support from the German Ministry of Education and Research (Center for Innovation Competence programme, grant 03Z1HN31), the Deutsche Forschungsgemeinschaft (grant NO462/6-1), the Thuringian Ministry for Education, Science and Culture (Research group Spacetime, grant 11027-514).

The authors declare that they have no competing financial interests.

Correspondence should be addressed to Max Tillmann (email: Max.Tillmann@univie.ac.at).